https://doi.org/10.17221/564/2025-PSE

Decoupling of stomatal and mesophyll recovery drives photosynthetic resilience to water deficit in sugar beet: evidence from multiscale structural and functional traits

Yangyang Li[1,2], Zengyuan Tian[1], Jixia Su[2], Kaiyong Wang[2], Pengpeng Zhang[3], Hua Fan[2]**

[1]*School of Agricultural Sciences, Zhengzhou University, Zhengzhou, Henan, P.R. China*
[2]*Agricultural College, Shihezi University, Shihezi, Xinjiang, P.R. China*
[3]*Institute for Crop Sciences, Chinese Academy of Agricultural Sciences, Beijing, P.R. China*
**Corresponding authors: pp_zhang0413@163.com; fanhua@shzu.edu.cn*

Citation: Li Y.Y., Tian Z.Y., Su J.X., Wang K.Y., Zhang P.P., Fan H. (2026): Decoupling of stomatal and mesophyll recovery drives photosynthetic resilience to water deficit in sugar beet: evidence from multiscale structural and functional traits. Plant Soil Environ., 72: 49–65.

Abstract: Water deficit severely constrains sugar beet productivity by impairing photosynthetic capacity. However, the underlying structure-function mechanisms conferring photosynthetic resilience remain poorly characterised. This study investigates the temporal dynamics of photosynthetic limitations and structural adaptations in sugar beet during water deficit and subsequent rehydration. We found that water deficit significantly reduced the maximum net CO_2 assimilation rate (A_{Nmax}) and the Rubisco carboxylation rate (V_{cmax}) by impairing CO_2 diffusion and biochemical processes. The reduction in photosynthetic capacity is primarily and stably attributed to mesophyll limitation, while contributions from stomatal and biochemical limitations flexibly change with deficit degree and rehydration. Severe water deficit caused irreversible structural damage that hinders recovery even after rehydration, while moderate water deficit allows partial restoration of leaf and chloroplast function. Partial least squares structural equation modelling (PLS-SEM) demonstrated that CO_2 diffusion was governed by the volume fraction of intercellular air space (f_{ias}, $\beta = 0.28$) and surface areas of the chloroplasts exposed to leaf intercellular air spaces (S_c/S, $\beta = 0.35$), with S_c/S indirectly influencing mesophyll conductance (g_m) through f_{ias} mediation ($\beta = 0.53$). Severe water deficit caused irreversible f_{ias} reduction and chloroplast interface damage (59% cell volume loss). These findings establish that resilience to water deficit in sugar beet depends on mesophyll structural integrity, with f_{ias} and S_c/S as key modulators of g_m recovery. The study advances understanding of stress recovery mechanisms in sugar beet and provides a framework for multiscale crop improvement in the context of climate change.

Keywords: sugar crop; stress condition; drought; chlorophyll; leaf thickness; chloroplast ultrastructure

Sugar beet (*Beta vulgaris* L.) is one of important sugar crops, which contributes to 30% of the total sugar production worldwide (Ghaffari et al. 2021). Over the past three decades, water deficit has been the primary limitation to sugar beet production (Brown et al. 1987, Bloch et al. 2006, Sahin et al. 2014, Shaaban et al. 2025), resulting in global yield losses of 10% to 50% (Fitters et al. 2022). With conventional agronomic approaches reaching their productivity limits (Flexas et al. 2025), improving photosynthetic performance under stress conditions has become crucial for sustaining yield stability (Flexas et al. 2025). Water deficit primarily limits photosynthesis by restricting CO_2 diffusion, a process fundamentally governed by leaf anatomical features (Flexas et al. 2012). However, while recent work has elucidated

Supported by the National Natural Science Foundation of China, Projects No. 32201700, 31771720, and 31660360.

https://doi.org/10.17221/564/2025-PSE

stomatal behavioural strategies (e.g., anisohydric response, light-triggered optimisation) for water use efficiency in sugar beet (Barratt et al. 2020), the structure-function dynamics underlying photosynthetic recovery, particularly the coordination between mesophyll anatomy and biochemical reactivation during rehydration, remain largely unresolved.

Photosynthetic limitation under water deficit operates through three interdependent pathways: stomatal closure (l_s), mesophyll conductance reduction (l_m), and biochemical impairment (l_b) (Grassi and Magnani 2005). Mechanistically, the decoupling of stomatal conductance (g_s) and mesophyll conductance (g_m) results in non-coordinated development of l_s and l_m under water deficit conditions (Flexas et al. 2012). Although stomatal regulation has been well-characterised (Tsai et al. 2022), the structural basis of l_m remains controversial. Crucially, under water deficit conditions, the l_m determined by g_m becomes the predominant and most significant photosynthetic limitation (Flexas et al. 2012, Zou et al. 2022). CO_2 diffusion from substomatal cavities to Rubisco active sites encounters: (*i*) gas-phase resistance through intercellular airspaces, and (*ii*) liquid-phase resistance across cell wall-chloroplast interfaces (Terashima et al. 2011). These structural parameters exhibit species-specific plasticity during drought recovery (Flexas et al. 2012).

In sugar beet, preliminary evidence suggests unique l_m regulation patterns (Sagardoy et al. 2010, Dohm et al. 2014). Unlike tobacco, where g_m recovers rapidly (Galle et al. 2009), or soybean, which shows irreversible g_m decline (Zou et al. 2022), sugar beet mesophyll may employ intermediate strategies, a hypothesis supported by its distinctive Kranz-like anatomy (Dohm et al. 2014). This anatomical specialisation potentially decouples l_m from l_s during rehydration, but the underlying structural dynamics remain unquantified. Furthermore, the relative contributions of key anatomical determinants (e.g., chloroplast repositioning, cell wall remodelling) to g_m recovery in sugar beet have not been systematically evaluated.

To address these knowledge gaps, we employed a multiscale approach integrating: (*i*) time-resolved partitioning of stomatal (l_s) and mesophyll (l_m) limitations; (*ii*) anatomical characterisation across scales, and (*iii*) mechanistic modelling *via* partial least squares structural equation modelling (PLS-SEM). We hypothesised that the capacity for photosynthetic recovery is governed by the degree of mesophyll structural preservation, with severe stress inducing irreversible damage to the chloroplast-airspace interface (S_c/S), the pivotal determinant of g_m resilience. By testing this framework, we aim to establish causal links between leaf anatomy and g_m recovery, advancing both the fundamental understanding of photosynthetic acclimation and the development of targeted breeding strategies for drought-resilient sugar beet.

MATERIAL AND METHODS

Plant material and water deficit treatments. Field trials were conducted in 2017 at the Agricultural College of Shihezi University, Xinjiang, China (45°20'N, 86°40'E), an arid continental region. The experimental soil was a Calcaric Fluvisol with a field capacity (FC) of 19% and a saturated water content (SWC) of 26%. The experiment comprised three distinct phases (see the timeline in Figure 1). Sugar beet (cultivar 356) was grown under standard irrigation until the canopy growth stage (defined as the period from the 9th to the 28th leaf expansion, a known water-sensitive period). During this sensitive stage, three constant soil-water regimes were imposed by daily gravimetric adjustment: (*i*) well-watered control (CK, 70% FC); (*ii*) moderate water deficit (M, 50% FC), and (*iii*) severe water deficit (S, 30% FC). Irrigation was triggered for a given plot when its soil water content fell to the specified lower limit of its treatment (i.e., 70, 50, or 30% of FC). At each irrigation event, water was applied to restore soil moisture to SWC. After the canopy growth stage ended, all plots, including the deficit treatments, were returned to the control irrigation schedule (70% FC) until harvest.

Gas exchange measurements. Gas exchange was measured on the same young, fully expanded main leaf per plant using a portable open-flow system (Li-6400xt; Li-Cor, Inc., Lincoln, USA). A standard, practical *in-situ* check for chamber integrity was implemented before measurements. Specifically, before and during measurements, the chamber gaskets were inspected, and a qualitative seal-check was performed. This involved gently applying positive pressure from a gas bag containing elevated CO_2 around the sealed IRGA chamber's gasket interface while monitoring the stability of the sample cell CO_2 concentration (C_{samp}). A stable C_{samp} reading during this procedure indicates an effective seal. For each treatment, three representative plants with 6–8 leaves

https://doi.org/10.17221/564/2025-PSE

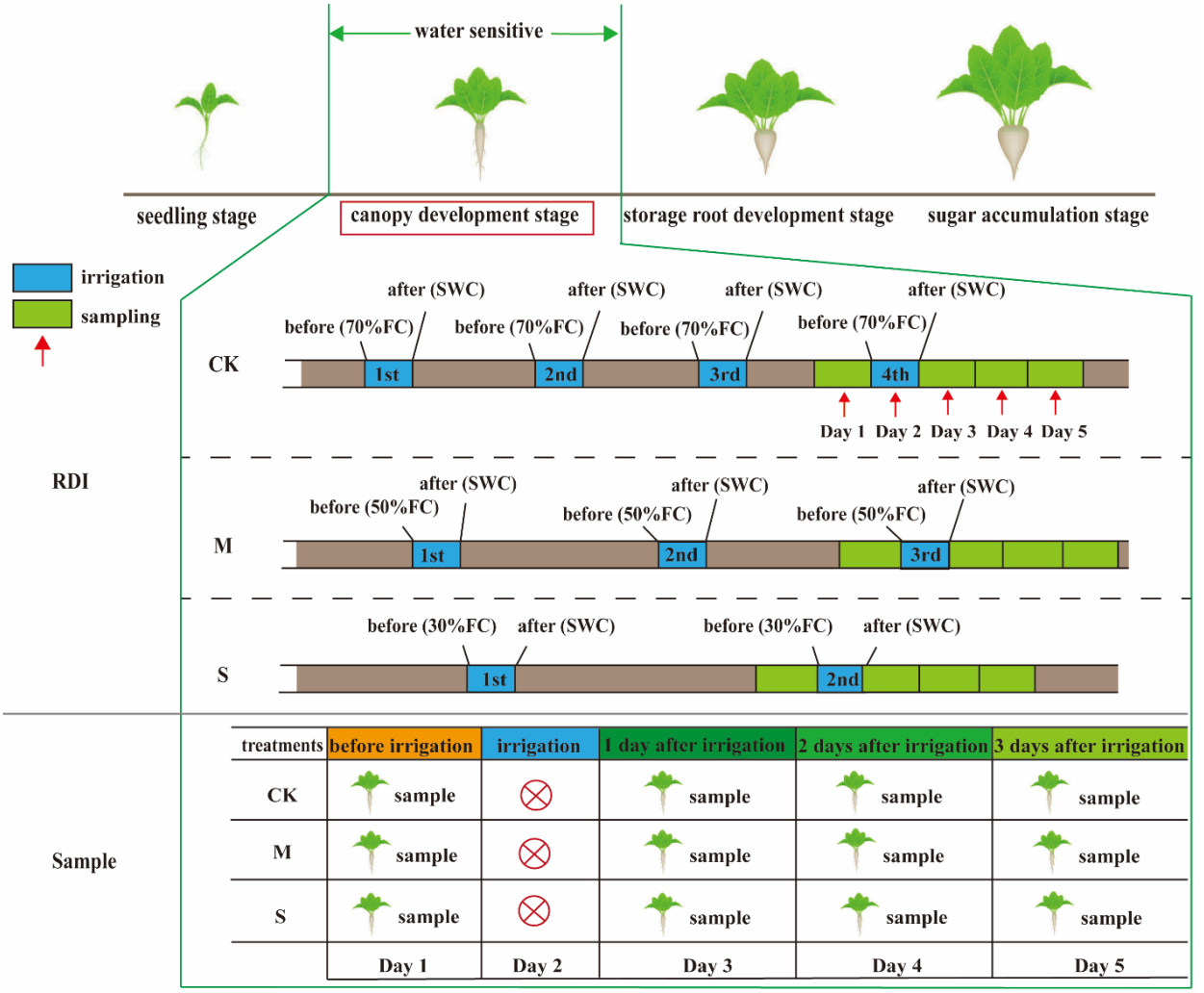

Figure 1. Three different regulated deficit irrigation (RDI) treatments i.e. control (CK), moderate deficit irrigation (M), and severe deficit irrigation (S) were set up during the canopy development stage. FC – field capacity; SWC – saturated water content. The blue rectangles represent the irrigation record and the green rectangles represent the sampling record

were selected. Light-response curves were generated by sequentially adjusting the photosynthetic photon flux density (PPFD) to 2 000, 1 800, 1 500, 1 200, 1 000, 800, 500, 300, 200, 150, 100, 50, and 0 μmol/m²/s. The reference CO_2 concentration in the leaf chamber (C_a) was maintained at 400 μmol/mol. At each PPFD level, measurements were recorded after net assimilation rate (A_N) and stomatal conductance (g_s) stabilised (typically 2–3 min). A non-rectangular hyperbola model (Farquhar et al. 1980) was fitted to derive the maximum net assimilation rate (A_{Nmax}) and apparent quantum efficiency (α). Following the light-response measurements on the same leaf, A_N-C_i curves were obtained at a saturating PPFD of 1 800 μmol/m²/s and a leaf temperature of 30 °C. The leaf chamber CO_2 concentration (C_a) was sequentially set to 400, 300, 200, 100, 50, 400, 600, 800, 1 000, 1 200, 1 500, and 1 800 μmol/mol. At each C_a step, gas exchange parameters were logged after full equilibration (typically 3–5 min per step, with the initial transition to 50 μmol/mol requiring ~30 min).

The maximum carboxylation rate of Rubisco (V_{cmax}) was estimated by fitting the Farquhar-von Caemmerer-Berry (FvCB) biochemical model (Farquhar et al. 1980) to the net assimilation rate *versus* chloroplastic CO_2 concentration (A_N-C_c) curves. The chloroplastic CO_2 concentration (C_c) was calculated as $Cc = C_i - A/g_m$, where C_i is the intercellular CO_2 concentration and g_m is the mesophyll conductance. The g_m value was simultaneously estimated from the same A-C_i curves using the variable J method (Harley et al. 1992), and dark respiration (R_d) was fitted as a free parameter

https://doi.org/10.17221/564/2025-PSE

during the nonlinear regression. This approach explicitly accounts for the finite and stress-sensitive g_m, thereby avoiding the substantial overestimation of V_{cmax} that occurs when g_m is assumed to be infinite (Flexas et al. 2012).

Chlorophyll fluorescence and estimation of mesophyll conductance. To complement the gas exchange measurements and to derive an independent estimate of electron transport rate for model parameterisation, chlorophyll fluorescence was measured on the same leaves used for the A_N-PPFD and A_N-C_i curves. Following a 30-min dark-adaptation period, a pulse-amplitude-modulated fluorometer (PAM-2500; Walz, Germany) was used. The quantum yield of photosystem II (ΦPSII) was determined at a series of actinic light intensities (0, 11, 36, 69, 106, 146, 203, 368, 624, 986, 1 165, and 1 391 μmol photons m^2/s). At each light level, measurements were taken after stabilisation (approximately 60 s).

The curve-fitting method introduced by Sharkey (2016) was used to obtain an alternative estimate of mesophyll conductance (g_m). This method was based on changes in the curvature of the A_N-C_i response curves owing to a finite g_m. By nonlinear curve fitting, minimising the sum of the squared model deviations from the data, g_m can be estimated from the observed data.

The quantum efficiency of the photosystem II photochemistry (ΦPSII) was calculated as follows:

$$\Phi_{PSII} = \frac{F_{m'} - F_s}{F_{m'}} \quad (1)$$

J_{flu} was then calculated as follows:

$$J_{flu} = \Phi_{PSII} \times PPFD \times \alpha \times \beta \quad (2)$$

where: PPFD – photosynthetically active photon flux density; α – leaf absorptance; β – partitioning of the absorbed quanta between photosystems II and I (PSI and PSII). α and β were assumed to be 0.85 and 0.5, respectively. These values represent standard estimates widely adopted for C_3 plants under non-stressed conditions (Von Caemmerer 2000) and have been applied in comparable studies on sugar beet (Sagardoy et al. 2010).

g_m was estimated using the variable J method (Harley et al. 1992) as follows:

$$g_m = \frac{A_N}{C_i - \frac{\Gamma^* \times \left[J_{flu} + 8\left(A_N + R_d\right)\right]}{J_{flu} - 4\left(A_N + R_d\right)}} \quad (3)$$

where: Γ* – CO_2 compensation point in the absence of mitochondrial respiration and is expressed as follows:

$$\Gamma^* = \exp\left(13.49 - \frac{24460}{8.314 \times (273.15 + T_L)}\right) \quad (4)$$

where: T_L – leaf temperature (°C); R_d – day respiration; A_N and C_i – obtained from gas exchange measurements under saturated light.

The calculated values of g_m were used to convert the A_N-C_i curves into A_N-chloroplast CO_2 concentration (C_c) curves using the following equation:

$$C_c = C_i - \frac{A_N}{g_m} \quad (5)$$

Electron microscopy. Leaf samples (1 × 1 cm) were cut from the upper part of sugar beet and immediately placed in FAA solution (5 mL of formaldehyde, 5 mL of glacial acetic acid, and 90 mL of 70% alcohol) and deposited in the refrigerator at 4 °C. For anatomical analysis, 8–10 samples were obtained and fixed; 3–5 fixed samples were selected for slice preservation, and all slices were measured to obtain the final data. The sections were prepared and photographed using an electron microscope (Zeiss Imager. M2, Germany); the photos were processed using Motic Imagers Advanced 3.2 software.

Leaf samples (1 × 4 mm) were cut from the same position and placed in a 2.5% glutaraldehyde fixative solution, which was then subjected to a vacuum to ensure that the samples sink. After 3 h, the samples were washed three times with 0.1 mol/L phosphate buffer and then transferred into 1% osmium acid for 2 h. The samples were washed three times with 0.1 mol/L phosphate buffer and dehydrated using acetone gradients of 30, 50, 70, 80, 90, and 100%. Sections were prepared using a LEICAUC 6 Ultrathin Slicer, which was double-stained with uranyl acetate and lead citrate. Sections of each sample were placed on a copper net, observed, and photographed using a JEM-1230 transmission electron microscope.

The surface areas of the mesophyll cells and chloroplasts exposed to leaf intercellular air spaces (S_m/S and S_c/S, respectively) were calculated as follows (Syvertsen et al. 1995):

$$\frac{S_m}{S} = \frac{L_{mes} \times F}{W} \quad (6)$$

$$\frac{S_c}{S} = \frac{L_c \times F}{W} \quad (7)$$

where: L_{mes} – total length of the mesophyll cells facing the intercellular air space in the palisade tissue section; L_c – total length of the chloroplast surface area facing the intercellular air space in mesophyll cells; F – curvature correction factor, which depends on the shape of the cells (Thain 1983, Evans et al. 1994); W – width of the section.

The volume fraction of intercellular air space (f_{ias}) was determined as follows:

https://doi.org/10.17221/564/2025-PSE

$$f_{ias} = 1 - \frac{\Sigma S_c}{t_{mes} \times W} \quad (8)$$

where: t_{mes} – mesophyll thickness between the two epidermal layers; ΣS_c – sum of the cross-sectional area of the mesophyll cells.

Chloroplast length (L_{chl}) and thickness (T_{chl}) were measured at different positions in each sample at × 30 000 magnifications. For a given section, all characteristics were determined using at least three different fields of view, and at least three different sections were analysed. As the cross-sections of chloroplasts are assumed to be oval, the cross-sectional area of the chloroplast ($Area_{chl}$) in the palisade or spongy tissue sections was calculated as follows:

$$Area_{chl} = \pi \times L_{chl} \times T_{chl} \quad (9)$$

where: π – ratio of the circumference of a circle to its diameter.

Relative limitation analyses on A_N. The relative limitations on A_N were analysed according to Grassi and Magnani (2005), including relative stomatal (l_s), mesophyll (l_m), and biochemical limitations (l_b). l_m was calculated using the g_m calculated from gas exchange and fluorescence measurements following (Harley et al. 1992). Anatomical characteristics were analysed using the model of Niinemets and Reichstein (2003) modified by Tosens et al. (2016). The relative changes in l_s, l_m, and l_b were calculated as follows:

$$l_s = \frac{\frac{g_{tot}}{g_s} \times \frac{\partial A_N}{\partial C_C}}{g_{tot} + \frac{\partial A_N}{\partial C_C}} \quad (10)$$

$$l_m = \frac{\frac{g_{tot}}{g_m} \times \frac{\partial A_N}{\partial C_C}}{g_{tot} + \frac{\partial A_N}{\partial C_C}} \quad (11)$$

$$l_b = \frac{g_{tot}}{g_{tot} + \frac{\partial A_N}{\partial C_C}} \quad (12)$$

where: g_{tot} – total conductance for CO_2 from the leaf surface to the carboxylation sites ($1/g_{tot} = 1/g_s + 1/g_m$); l_s, l_m, and l_b – corresponding relative limitations ($0 < l_i < 1$, i = s, m, b). $\partial A_N/\partial C_c$ was calculated as the slope of the A_N-C_i response curve over a C_c range of 50–100 μmol/mol (Tomás et al. 2013). The l_s, l_m, and l_b were first calculated at the level of the individual biological replicate. Treatment means and measures of variation (e.g., standard error) were then computed from these replicate-level values.

Structural equation modeling. Partial least squares structural equation modeling (PLS-SEM) was conducted to quantify the direct and indirect effects of leaf structural traits on mesophyll conductance (g_m). All indicators were standardised prior to analysis. Model specification and estimation were performed using SmartPLS 4.0 (Hair et al. 2022) with the path weighting scheme and a maximum of 300 iterations. Discriminant validity *via* Fornell-Larcker criterion. The significance of path coefficients was evaluated using bootstrapping with 5 000 resamples (two-tailed test).

Statistical analysis. Data were analysed using SPSS (version 12.0, IBM Corp., Armonk, USA). Prior to parametric analysis, the underlying assumptions were verified: normality of residuals was assessed using the Shapiro-Wilk test, and homogeneity of variances was checked with Levene's test. For data that violated these assumptions, an appropriate logarithmic transformation was applied. If the transformed data still did not meet the assumptions, the non-parametric Kruskal-Wallis test was used instead of ANOVA. For one-way ANOVA with a significant overall effect ($P < 0.05$), Duncan's new multiple range test was employed for post-hoc pairwise comparisons among treatment means. All results are presented as mean ± standard error (SE). Figures were generated using Origin (Version 8.5, OriginLab Corp., Northampton, USA).

Data availability. Raw data were generated using LI-6400/XT (LI-COR, Lincoln, USA), PAM-2500 (WALZ, Effeltrich, Germany), and CX33 (OLYMPUS, Tokyo, Japan). Data supporting the findings of this study are available from the corresponding author (fanhua@shzu.edu.cn) upon request.

RESULTS

Photosynthetic responses to water deficit and rehydration. The photosynthetic response of A_N to PPFD showed significant differences on Day 1, but the response curves became highly consistent on Days 3, 4, and 5 under varying soil water deficit conditions (Figure 2). On Day 1, the photosynthetic rate increased with PPFD in all treatments, with the CK treatment having the highest rate, followed by M and then S. By Day 3 and 4, the photosynthetic rates had increased across three water deficit treatments, although the CK treatment still had the highest rates, but the differences among treatments were less significant. By Day 5, the photosynthetic rates had further increased for three water deficit treatments, with the CK treatment still maintaining the highest rates. Overall, the CK treatment consistently supported higher photosynthetic rates across different PPFD levels and days.

https://doi.org/10.17221/564/2025-PSE

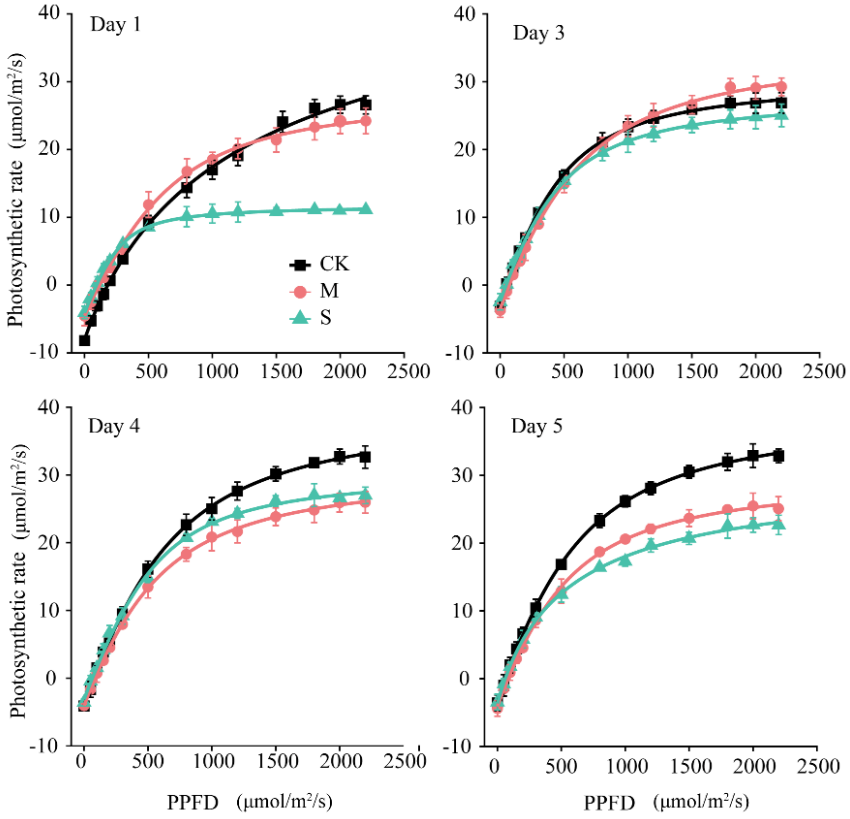

Figure 2. Photosynthetic rate expressed on the basis of photosynthetic photon flux density (PPFD) for control (CK), moderate deficit irrigation (M), and severe deficit irrigation (S) treatments on Day 1, Day 3, Day 4, and Day 5

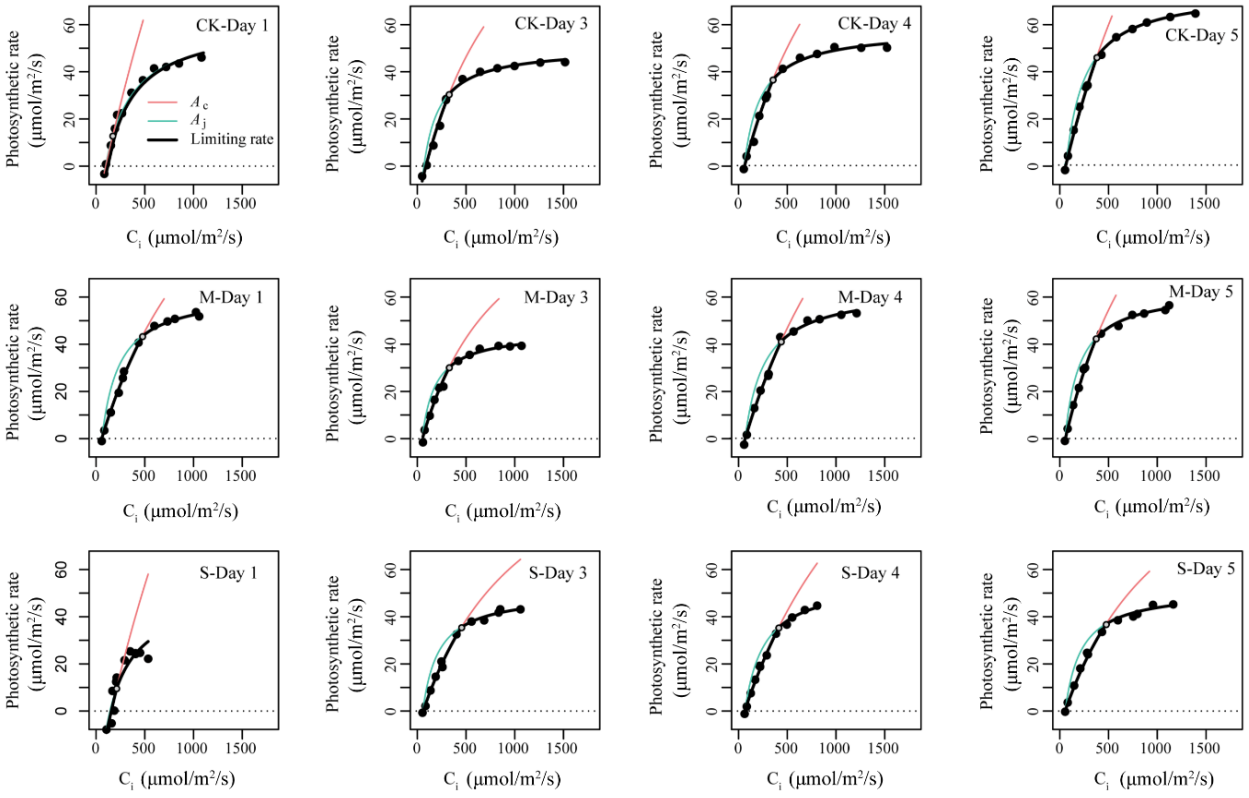

Figure 3. Photosynthetic rate expressed on the basis of intercellular CO_2 concentration (C_i) for control (CK), moderate deficit irrigation (M), and severe deficit irrigation (S) treatments on Day 1, Day 3, Day 4, and Day 5

https://doi.org/10.17221/564/2025-PSE

Table 1. Comparison of maximum net photosynthetic rate (A_{Nmax}) parameters from light response curves, maximum carboxylation efficiency (V_{cmax}) parameters from CO_2 response curves, and their coefficients of variation among control (CK), moderate deficit irrigation (M), and severe deficit irrigation (S) treatments

Treatment	A_{Nmax} (μmol/m²/s)				V_{cmax} (μmol/m²/s)			
	Day 1	Day 3	Day 4	Day 5	Day 1	Day 3	Day 4	Day 5
CK	33.30 ± 5.26	30.40 ± 2.92	36.15 ± 0.96	38.02 ± 3.27	48.62 ± 3.36	45.93 ± 1.54	57.05 ± 5.85	60.94 ± 3.21
M	27.35 ± 0.92*	31.64 ± 1.91	27.61 ± 1.77*	28.49 ± 1.28*	47.62 ± 6.05	47.21 ± 2.38	51.43 ± 6.29	57.25 ± 2.00
S	13.63 ± 2.19**	20.55 ± 3.21*	28.45 ± 2.09*	25.96 ± 2.20*	24.30 ± 1.17**	45.14 ± 2.88	47.43 ± 2.57*	49.61 ± 4.25*
CV (%)	26.99				19.43			

The photosynthetic response of A_N to C_i initially increased with rising C_i levels, eventually reaching a plateau, which indicates the saturation point of photosynthesis (Figure 3). Under the CK condition, A_N exhibited a pronounced increase from Day 1 to Day 5, reflecting enhanced photosynthetic efficiency following rehydration. A similar trend was observed in the M condition, although its plateau occurred at a slightly lower C_i, indicating reduced photosynthetic efficiency. In contrast, the S condition showed a slower increase in A_N, with the plateau occurring at the lowest C_i level, suggesting impaired photosynthetic capacity. Additionally, the apparent photosynthetic rate (A_j) was generally lower than the actual photosynthetic rate (A_c) under the three water deficit conditions, suggesting that photorespiration or other limiting factors were influencing the photosynthetic process.

From Day 1 to Day 5, all three treatments showed increases in both the maximum net CO2 assimilation rate (ANmax) and the maximum Rubisco carboxylation rate (V_{cmax}). A_{Nmax} generally increased across the three treatments from Day 1 to Day 5, with initial values of 33.30, 27.35, and 13.63 μmol/m²/s

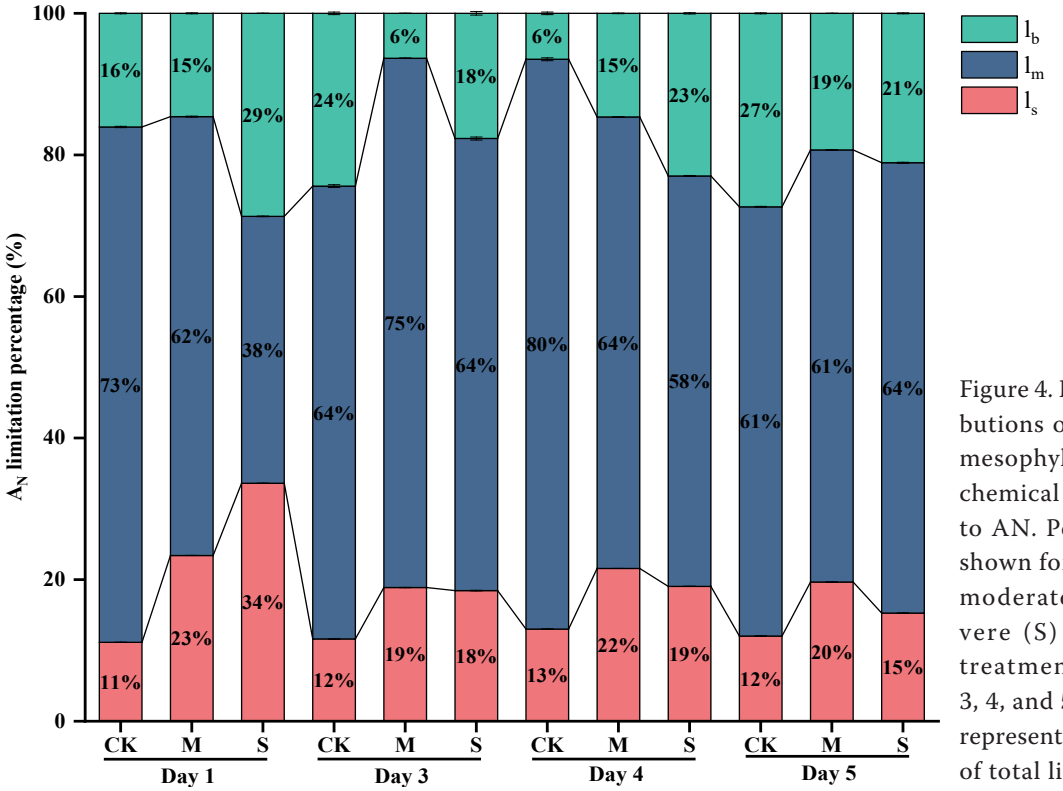

Figure 4. Relative contributions of stomatal (l_s), mesophyll (l_m), and biochemical (l_b) limitations to AN. Percentages are shown for control (CK), moderate (M), and severe (S) water deficit treatments on Days 1, 3, 4, and 5. These values represent the proportion of total limitation

https://doi.org/10.17221/564/2025-PSE

Table 2. Absolute photosynthetic limitations under different water deficit treatments

Treatment	Photosynthetic limitations (μmol/m^2/s)			
	Day 1	Day 3	Day 4	Day 5
CK	11.60 ± 0.081	2.34 ± 0.004	7.31 ± 0.001	4.52 ± 0.001
M	1.68 ± 0.005**	10.11 ± 0.015**	0.22 ± 0.000**	4.07 ± 0.001
S	1.20 ± 0.002**	1.92 ± 0.001*	9.64 ± 0.005*	1.93 ± 0.000*

CK – control; M – moderate deficit irrigation; S – severe deficit irrigation

under CK, M, and S treatments, respectively, and reaching 38.02, 28.49, and 25.96 μmol/m^2/s on Day 5. Similarly, V_{cmax} for the CK, M, and S treatments increased from 48.62, 47.62, and 24.30 μmol/m^2/s to 60.94, 57.25, and 49.61 μmol/m^2/s, respectively. The coefficient of variation (CV) for A_{Nmax} and V_{cmax} was 26.99% and 19.43%, respectively, indicating that measurements of A_{Nmax} were more variable than those of V_{cmax} (Table 1).

Temporal dynamics analysis of photosynthetic limitations. On Day 1, the relative contribution of stomatal limitation (l_s) to the total limitation of A_N was highest in the S treatment, intermediate in M, and lowest in CK (Figure 4). Concomitantly, the absolute value of l_s also increased with stress severity. In contrast, the relative contribution of mesophyll limitation (l_m) exhibited an inverse pattern, constituting the majority (> 65%) of the total limitation across all treatments. From Day 3 to Day 5 during rehydration, the proportion of l_s remained nearly unchanged in the CK treatment. In contrast, both M and S treatments showed a reduction in the relative proportion of l_s, indicating a shift in the partitioning of limitations post-irrigation. Biochemical limitation (l_b) displayed a dynamic response: it was highest in the S treatment on Day 1, decreased in both M and S treatments on Days 3 and 4, but by Day 5, its relative proportion had increased again to a considerable level in the S treatment. This late increase in the proportion of l_b under severe stress occurred alongside persistently high absolute limitations, suggesting a progressive failure of biochemical recovery mechanisms. These proportional shifts (Figure 4) occurred alongside a substantial increase in the absolute magnitude of each limitation under water deficit. The absolute values of l_s, l_m, and l_b limitations, which quantify the actual constraint on CO_2 assimilation (Table 2).

Stomatal limitation (l_s) exhibited a highly significant negative correlation with g_s in the CK ($P < 0.05$), M ($P < 0.001$), and S ($P < 0.001$) treatments, indicating that the contribution of l_s to photosynthetic rate was directly dependent on stomatal behaviour (Figure 5). Similarly, l_m showed a strongly negative relationship with g_m in both CK and M treatments ($P < 0.01$). However, the l_m–g_m correlation weakened substantially under S treatment, where three outliers suggested the emergence of non-diffusional limitations under extreme water stress (Figure 5).

Temporal modifications in leaf and chloroplast architecture. On Day 1, the S treatment exhibited significant increases in leaf thickness, mesophyll thickness, and mesophyll cell area by 15, 7, and 17%, respectively, compared to the CK treatment (Figure 6, Table 3). Conversely, the mesophyll cell volume in the

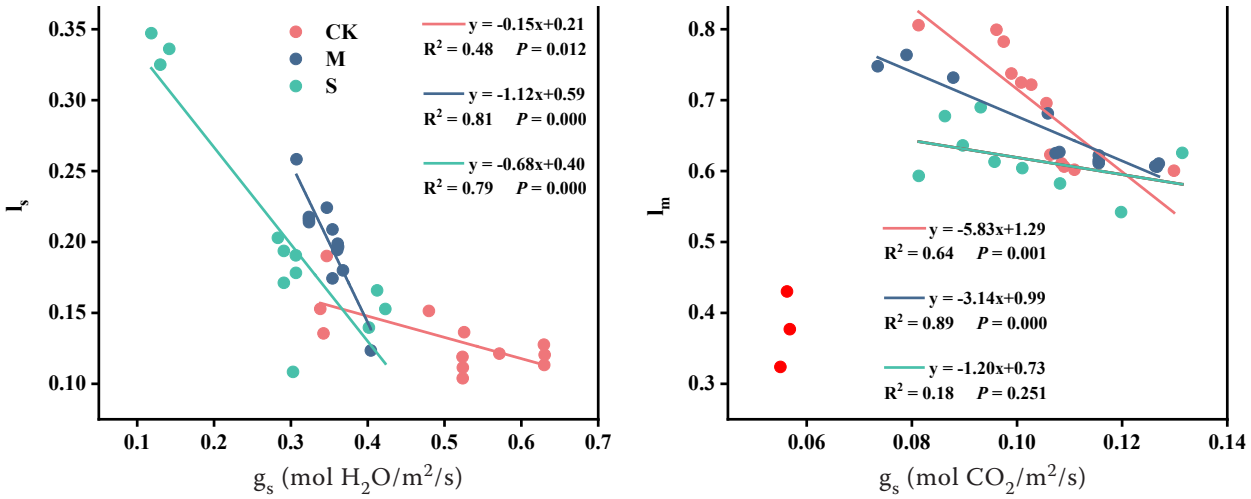

Figure 5. Relationships between photosynthetic limitations and conductance, and statistical validation of slope differences. CK – control; M – moderate deficit irrigation; S – severe deficit irrigation

https://doi.org/10.17221/564/2025-PSE

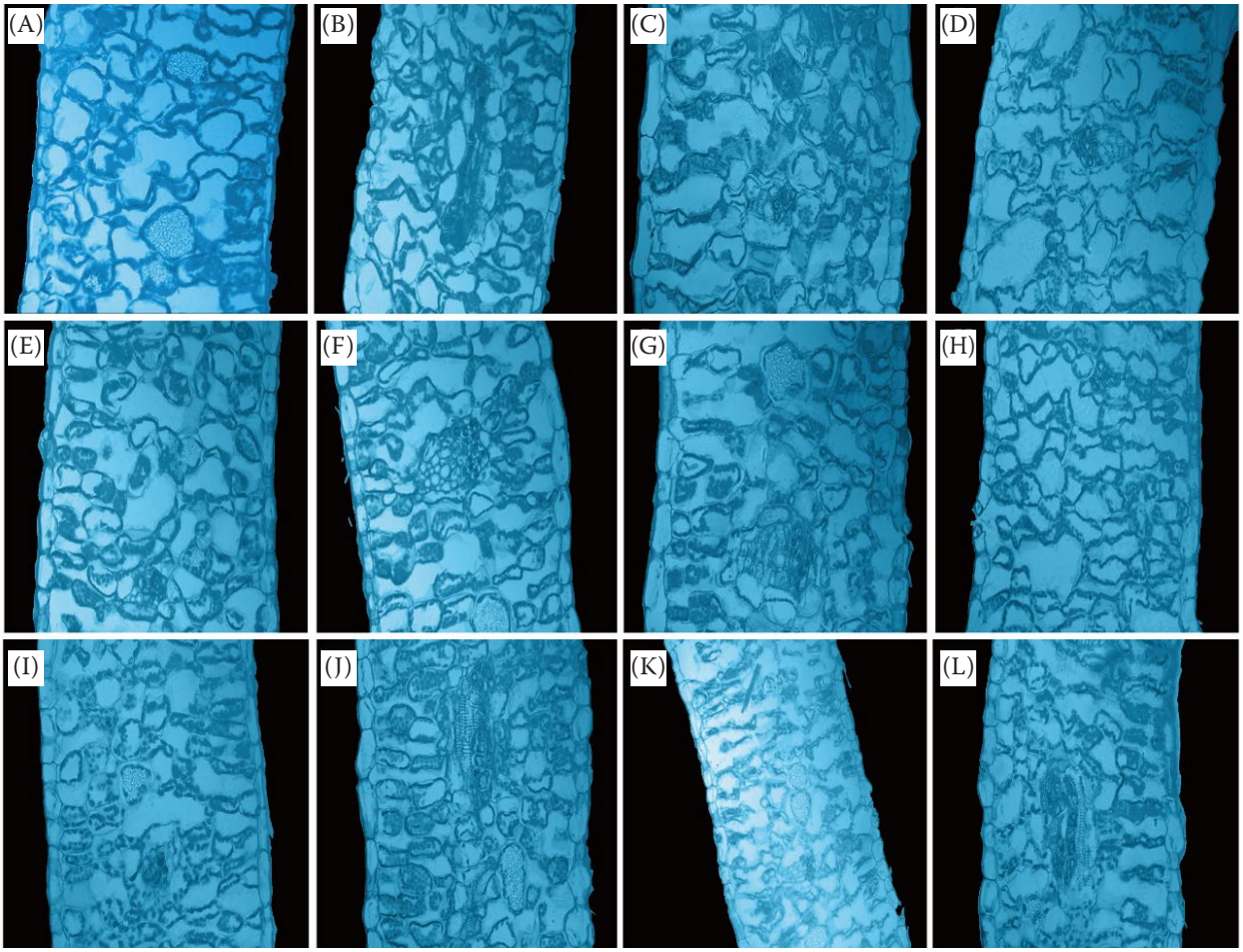

Figure 6. Microstructural dynamics of sugar beet leaves across water deficit and rehydration phase. (A–D) display the microstructure of leaves from the control (CK) treatment on Day 1 (A), Day 3 (B), Day 4 (C), and Day 5 (D). (E–H) depict the microstructural changes in leaves subjected to moderate water deficit (M) on Day1 (E), Day 3 (F), Day 4 (G), and Day5 (H). (I–L) capture the leaf microstructure under severe water deficit (S) on Day1 (I), Day 3 (J), Day 4 (K), and Day5 (L)

M treatment decreased significantly by 33% relative to the CK treatment. Additionally, the S_c/S and f_{ias} in the M and S treatments decreased significantly by 10% and 23%, and 15% and 21%, respectively, compared to the CK treatment. Following irrigation on Day 3, the M treatment showed significant increases in leaf thickness, mesophyll thickness, and mesophyll cell area of 7, 11, and 26%, respectively, compared with the CK treatment. In contrast, the S treatment exhibited a significant increase in mesophyll cell volume by 38% relative to the CK treatment, while S_c/S and f_{ias} decreased significantly by 14% and 13%, respectively, compared to the CK treatment. On Day 4, the S treatment displayed significant decreases in leaf thickness, mesophyll thickness, mesophyll cell area, mesophyll cell volume, the S_m/S, S_c/S, and f_{ias} by 29, 28, 50, 59, 26, and 19%, respectively, compared to the CK treatment. Moreover, the f_{ias} in both the M and S treatments decreased significantly compared to the CK treatment. By Day 5, leaf thickness, mesophyll thickness, mesophyll cell area, and S_m/S in the M and S treatments decreased significantly, while S_c/S and f_{ias} increased significantly compared to the CK treatment.

On Day 1, the M treatment exhibited a reduction of approximately 21% in chlorophyll ($a + b$) content, while the S treatment experienced a more pronounced decrease of about 52% in chlorophyll ($a + b$) and a 53% decline in the chlorophyll a/b ratio (Table 4). The chloroplast number in the M and S treatments significantly decreased by 38% and 40%, respectively, compared to the CK treatment. The $Area_{chl}$ in the M treatment significantly decreased by 13% and 16% compared to the CK and S treatments,

https://doi.org/10.17221/564/2025-PSE

Table 3. Leaf thickness, leaf mesophyll thickness, mesophyll cell area, mesophyll cell volume, the cross-sectional areas of mesophyll cells and chloroplasts exposed to leaf intercellular airspaces (S_m/S and S_c/S; $\mu m^2/\mu m^2$), the volume fraction of intercellular air space (f_{ias}) under CK, M and S treatments on Day 1, Day 3, Day 4, and Day 5

Treatment		Leaf thickness (μm)	Leaf mesophyll thickness (μm)	Mesophyll cell area (μm^2)	Mesophyll cell volume (μm^3)	S_m/S	S_c/S	f_{ias} (%)
Day 1	CK	0.46 ± 0.009	0.41 ± 0.003	0.36 ± 0.013	0.021 ± 0.006	1.17 ± 0.024	0.60 ± 0.017	0.53 ± 0.005
	M	0.47 ± 0.026	0.41 ± 0.017	0.33 ± 0.018	0.014 ± 0.003*	1.15 ± 0.015	0.54 ± 0.016*	0.45 ± 0.016*
	S	0.53 ± 0.009*	0.44 ± 0.019*	0.42 ± 0.022*	0.023 ± 0.005	1.22 ± 0.043	0.46 ± 0.007*	0.42 ± 0.005*
Day 3	CK	0.46 ± 0.003	0.38 ± 0.031	0.31 ± 0.012	0.016 ± 0.004	0.88 ± 0.007	0.65 ± 0.025	0.52 ± 0.008
	M	0.49 ± 0.020*	0.42 ± 0.017*	0.39 ± 0.018*	0.020 ± 0.001	1.01 ± 0.045	0.71 ± 0.009	0.57 ± 0.010
	S	0.48 ± 0.027	0.41 ± 0.020	0.37 ± 0.017	0.022 ± 0.004*	1.01 ± 0.044	0.56 ± 0.023*	0.45 ± 0.005*
Day 4	CK	0.58 ± 0.021	0.50 ± 0.010	0.52 ± 0.024	0.027 ± 0.002	1.14 ± 0.045	0.62 ± 0.004	0.53 ± 0.022
	M	0.57 ± 0.009	0.50 ± 0.013	0.51 ± 0.012	0.023 ± 0.007	1.13 ± 0.030	0.59 ± 0.016	0.47 ± 0.031*
	S	0.41 ± 0.017*	0.36 ± 0.018**	0.26 ± 0.002**	0.011 ± 0.003**	0.84 ± 0.018*	0.50 ± 0.017*	0.46 ± 0.014*
Day 5	CK	0.63 ± 0.016	0.54 ± 0.007	0.56 ± 0.021	0.020 ± 0.002	1.40 ± 0.014	0.53 ± 0.016	0.47 ± 0.012
	M	0.51 ± 0.006*	0.44 ± 0.011*	0.40 ± 0.021*	0.018 ± 0.001	1.07 ± 0.011*	0.59 ± 0.012*	0.51 ± 0.013*
	S	0.43 ± 0.018**	0.39 ± 0.005*	0.31 ± 0.030*	0.015 ± 0.004	1.05 ± 0.015*	0.61 ± 0.013*	0.56 ± 0.012*

Table 4. Chlorophyll *a* + *b* (chl (*a* + *b*)), the ratio between chlorophyll *a* and chlorophyll *b* (chl *a*/*b*), chloroplast number, chloroplast length and chloroplast thickness and the cross-section area of chloroplast ($Area_{chl}$) under CK, M and S treatments by the Day 1, Day 3, Day 4, and Day 5

Treatment		Chl (*a* +*b*) (mg/L)	Chl *a*/*b* (%)	Chloroplast number	Chloroplast length (μm)	Chloroplast thickness (μm)	$Area_{chl}$ (μm^2)
Day 1	CK	21.74 ± 2.52	2.52 ± 0.23	20.00 ± 3.61	6.42 ± 0.19	2.41 ± 0.13	48.31 ± 7.05
	M	17.10 ± 2.45*	2.45 ± 0.38	12.33 ± 2.52*	5.75 ± 0.30	2.32 ± 0.17	41.97 ± 5.14*
	S	10.38 ± 1.18**	1.18 ± 0.01*	12.00 ± 1.58*	5.54 ± 0.31	2.87 ± 0.16	49.98 ± 5.86
Day 3	CK	16.64 ± 1.97	1.97 ± 0.07	12.00 ± 1.13	6.33 ± 0.55	2.61 ± 0.14	52.25 ± 6.92
	M	16.20 ± 2.31	2.31 ± 0.21*	10.33 ± 1.06	5.77 ± 0.67	2.32 ± 0.18	42.13 ± 6.74*
	S	11.32 ± 1.76*	1.75 ± 0.19	13.33 ± 1.53	6.17 ± 0.78	2.45 ± 0.28	47.06 ± 3.28*
Day 4	CK	17.06 ± 2.11	2.11 ± 0.18	14.67 ± 2.03	5.64 ± 0.43	2.39 ± 0.13	42.10 ± 8.57
	M	15.26 ± 2.27	2.27 ± 0.10	18.00 ± 1.12*	5.65 ± 0.11	2.25 ± 0.11	39.86 ± 3.09
	S	19.03 ± 2.39	2.39 ± 0.05	17.67 ± 1.53*	5.85 ± 0.44	1.89 ± 0.13*	37.79 ± 3.66*
Day 5	CK	12.73 ± 2.31	2.31 ± 0.13	10.67 ± 1.50	6.13 ± 0.21	3.14 ± 0.06	60.69 ± 7.34
	M	13.02 ± 2.27	2.27 ± 0.16	9.33 ± 0.58	7.81 ± 0.38*	2.37 ± 0.08*	58.11 ± 4.49*
	S	17.25 ± 2.19*	2.18 ± 0.13	8.33 ± 0.24*	5.04 ± 0.18*	2.90 ± 0.12*	46.01 ± 7.68**

https://doi.org/10.17221/564/2025-PSE

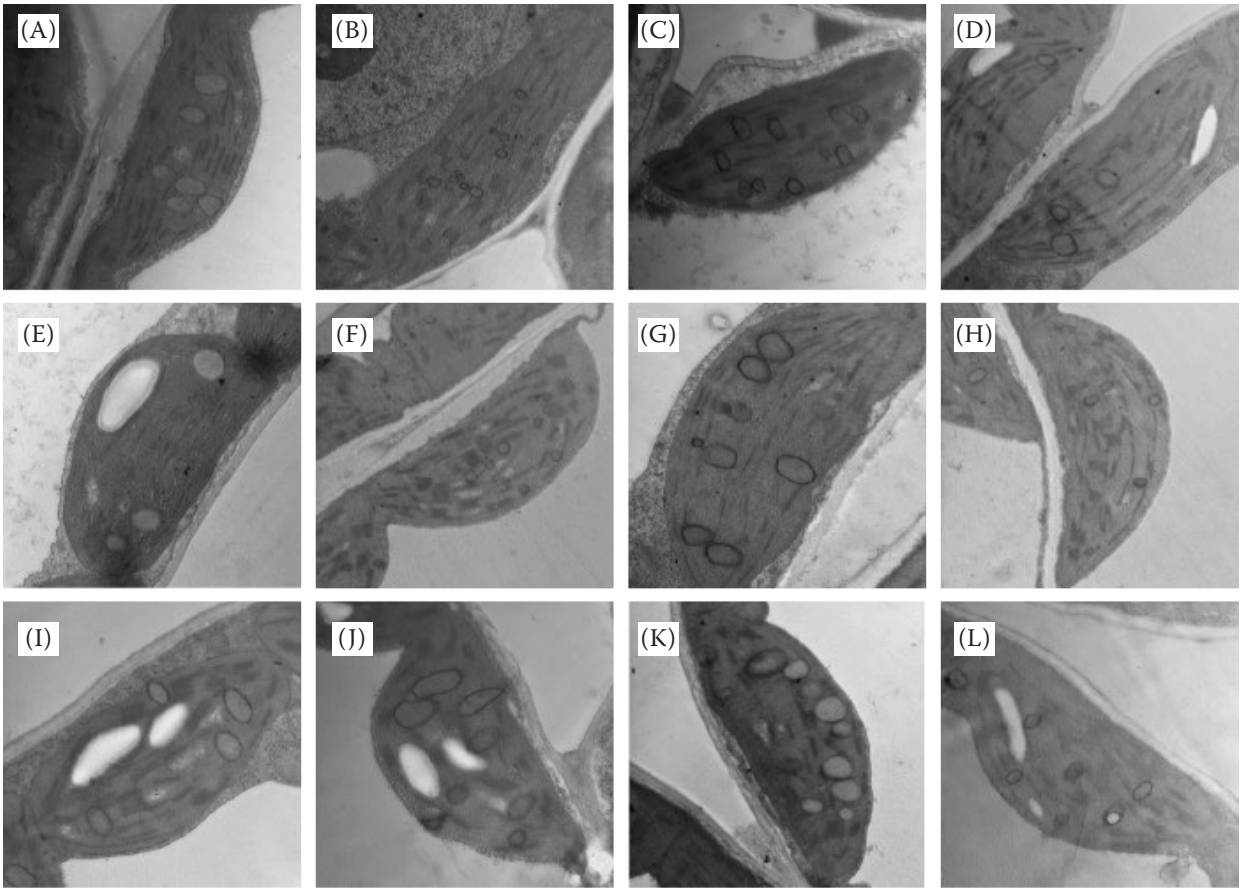

Figure 7. Chloroplast ultrastructure in sugar beet under different water treatments. (A–D) display the chloroplast ultrastructure on Day 1 (A), Day 3 (B), Day 4 (C), and Day 5 (D) under the control (CK) treatment. (E–H) show the changes in chloroplast ultrastructure on Day 1 (E), Day 3 (F), Day 4 (G), and Day 5 (H) under moderate (M) water deficit. (I–L) capture the chloroplast ultrastructure on Day 1 (I), Day 3 (J), Day 4 (K), and Day 5 (L) under severe (S) water deficit

respectively. On Day 3, the S treatment showed a substantial decrease in chlorophyll ($a + b$) content by 32% compared to the CK treatment. The chlorophyll a/b ratio increased by 17% in the M treatment, while $Area_{chl}$ decreased by 19% compared to the CK treatment. On Day 4, chloroplast numbers in the M and S treatments increased by 23% and 20%, respectively, compared to the CK treatment. The chloroplast thickness and $Area_{chl}$ in the S treatment significantly decreased by 21% and 10%, respectively, compared to the CK treatment (Figure 7, Table 4). By Day 5, the S treatment demonstrated an increase in chlorophyll ($a + b$) content by about 26% compared to the CK treatment. The chloroplast number in the S treatment significantly decreased by approximately 22% compared to the CK treatment. Furthermore, the length, thickness, and S_c/S in the S treatment were reduced by 15, 12, and 23%, respectively, compared to those in the CK treatment.

Structural determinants of g_m. The scatterplots reveal significant correlations between g_m and several structural indicators, including leaf thickness, mesophyll thickness, S_m/S, mesophyll cell area, mesophyll cell volume, f_{ias}, chloroplast number, chloroplast length, chloroplast thickness, chloroplast area, and S_c/S (Figure 8). The relationship between g_m and f_{ias} reveals a positive correlation, suggesting that an increase in f_{ias} is associated with an enhancement in g_m. The relationship between g_m and S_c/S also shows a positive correlation. The positive correlation between g_m and structural indicators including f_{ias} and S_c/S underscores the importance of optimising intercellular air space structure to improve photosynthetic efficiency.

The partial least squares structural equation modelling (PLS-SEM) demonstrates a direct positive effect of the S_c/S on g_m, with a standardised path coefficient (β) of 0.35 ($P < 0.01$). Additionally, the PLS-SEM reveals a direct positive effect of the f_{ias} on g_m, with a standard-

https://doi.org/10.17221/564/2025-PSE

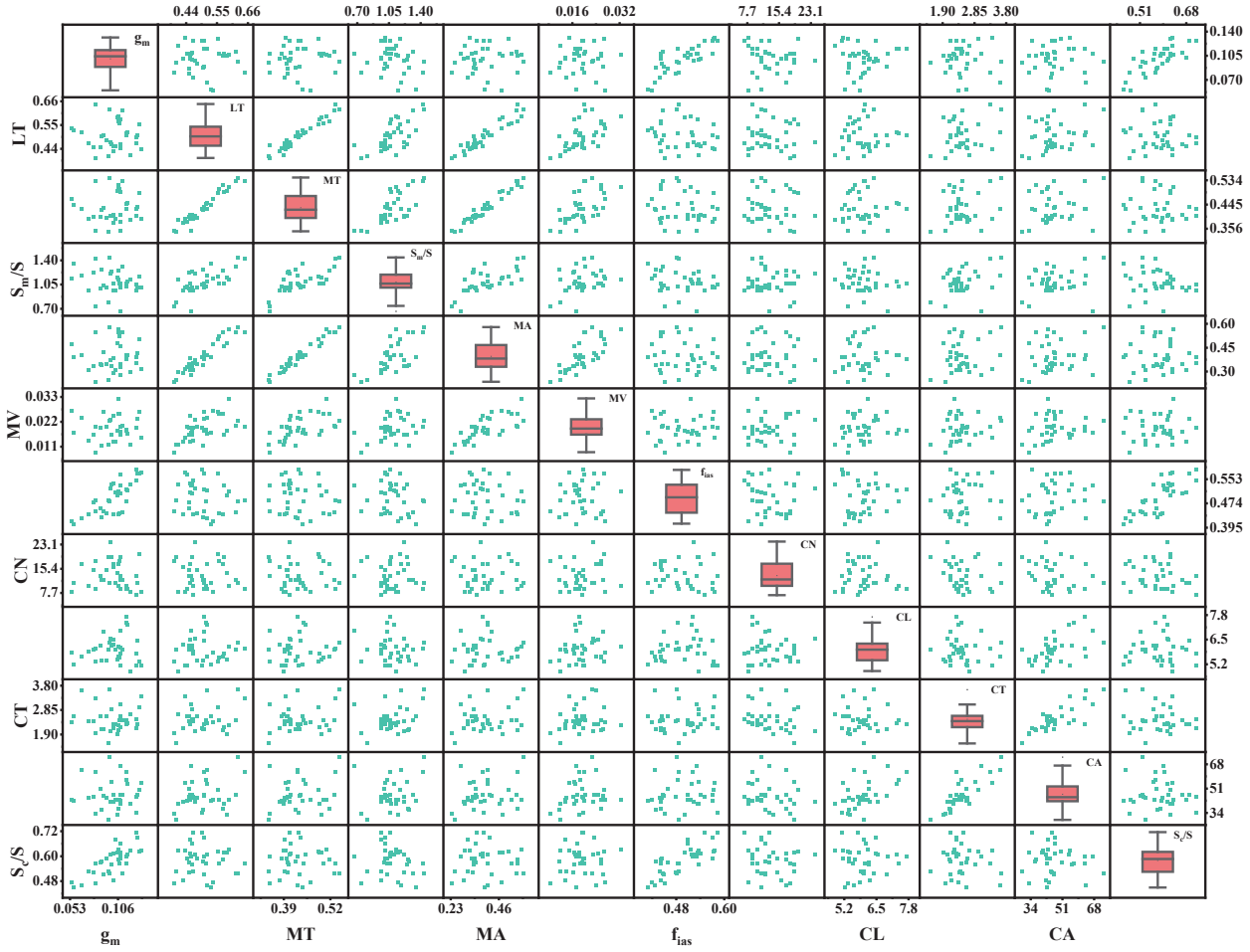

Figure 8. Scatterplot matrix showing the relationships between mesophyll conductance (gm) and leaf thickness (LT), mesophyll thickness (MT), the cross-sectional areas of mesophyll cells exposed to leaf intercellular airspaces (S_m/S), mesophyll cell area (MA), mesophyll cell volume (MV), the volume fraction of intercellular air space (f_{ias}), chloroplast number (CN), chloroplast length (CL), chloroplast thickness (CT), chloroplast area (CA), the cross-sectional areas of chloroplasts exposed to leaf intercellular airspaces (S_c/S)

ised path coefficient (β) of 0.28 ($P < 0.01$). Furthermore, the PLS-SEM indicates an indirect effect of S_c/S on g_m mediated through f_{ias}. The path coefficient from S_c/S to f_{ias} is β = 0.63 ($P < 0.01$). The product of these path coefficients (0.63 × 0.28) yields an indirect effect of 0.18, suggesting that changes in S_c/S can indirectly influence g_m through its effect on f_{ias}. The total effect of S_c/S on g_m is the sum of the direct effect (0.35) and the indirect effect (0.18), resulting in a total effect of approximately 0.53. This indicates that a significant portion of the influence of S_c/S on g_m is mediated through f_{ias} (Figure 9).

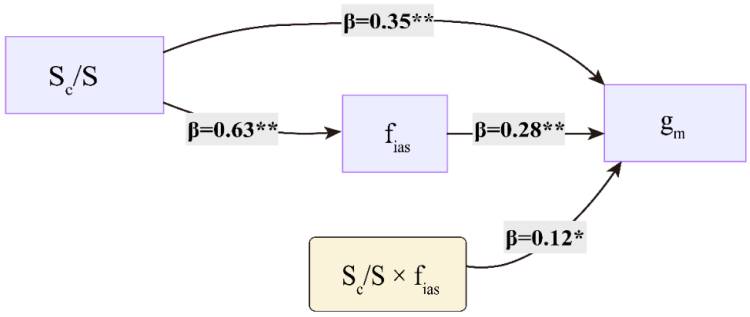

Figure 9. Partial least squares structural equation modeling (PLS-SEM) depicting effects of the surface of chloroplasts exposed to leaf intercellular airspaces (S_c/S) and the volume fraction of intercellular air space (f_{ias}) on mesophyll conductance (g_m) in sugar beet. *$P < 0.05$; **$P < 0.01$

https://doi.org/10.17221/564/2025-PSE

DISCUSSION

Photosynthetic limitations under water deficit-rehydration: decoupling of stomatal and mesophyll recovery. Photosynthetic acclimation to water stress and rehydration involves complex coordination between diffusional and biochemical processes (Flexas and Carriquí 2020). In this study, both M and S water deficits significantly decreased A_{Nmax} and V_{cmax} in sugar beet (Table 1), indicating that water deficit directly affects the ability of sugar beet leaves to capture and utilise CO_2 (Zou et al. 2022). Although rehydration improved A_{Nmax} and V_{cmax} in the M and S treatments, their inability to attain the levels observed in the CK treatment (Table 1), in conjunction with the sustained reductions in f_{ias} and S_c/S (Table 3), indicates that long-term or partially irreversible constraints persisted in the photosynthetic apparatus (Flexas and Carriquí 2020). The persistent predominance of l_m during the recovery phase (Figure 4) suggests that these constraints were strongly associated with limitations in CO_2 diffusion and carboxylation. The observed reduction in V_{cmax}, evidenced by a low coefficient of variation (19.43%) across treatments (Table 1), is consistent with a sustained biochemical limitation. This could be explained by several non-exclusive mechanisms, including a reduction in Rubisco content or activation state, limitations in RuBP regeneration capacity, or downstream metabolic impairments (Yamori et al. 2006). In the absence of direct measurements of Rubisco activity or content, we cannot definitively pinpoint the primary biochemical lesion; however, the stability of the V_{cmax} depression points toward alterations in the carboxylation machinery rather than transient regulatory adjustments.

Notably, l_m dominated water deficit and rehydration stages in sugar beet in relative terms (Figure 4), providing a direct explanation for the severe suppression of A_N under stress. This contrasts with *Vitis*, where l_s and l_m balanced during acclimation (Flexas et al. 2009). This difference reveals species-specific coordination patterns between stomatal and mesophyll responses. In sugar beet, the sustained dominance of l_m may prioritise the maintenance of mesophyll structure under stress, potentially facilitating post-drought recovery at the cost of immediate photosynthetic carbon gain (Chaves et al. 2009). In grapevine, a stronger coupling between l_s and l_m aligns with its pronounced stomatal sensitivity to water potential, a key component of embolism avoidance in woody species (Flexas et al. 2009). Both M and S treatments enhanced the control of g_s over l_s, as evidenced by steeper regression slopes (Figure 5). This indicates a sensitised stomatal response to prioritise water conservation (Velikova et al. 2018). Concurrently, the absolute stomatal limitation increased significantly, contributing substantially to the total A_N reduction. The slope of l_m–g_m regression under CK (–5.83) and M (–3.14) reflects a progressive loss of mesophyll compensatory capacity (Figure 5). This was paralleled by a dramatic rise in the absolute l_m, which became the largest single component restricting A_N under severe stress. In the S treatment, although l_s remained tightly coupled to g_s, l_m became increasingly dominated by non-diffusional factors. The decoupling of l_m from g_m, alongside its high absolute value, demonstrates that stomatal behaviour operated independently of a mesophyll function that was severely and persistently constrained, both structurally and biochemically (Flexas et al. 2012). When interpreting the magnitude of l_m, it should be noted that the calculation of C_i in this study relied on g_s. Under severe water deficit, when stomatal aperture is minimal, unaccounted cuticular conductance may lead to a slight overestimation of C_i. This, in turn, could result in a conservative estimate of the reduction in g_m and l_m. Future studies incorporating direct measurements of cuticular conductance would refine the accuracy of partitioning diffusional limitations under extreme drought conditions.

Structural adaptation in response to water deficit-rehydration. The observed cellular responses to water deficit and rehydration reveal distinct patterns of structural adaptation and recovery limitations. Notably, the S treatment induced significant cellular expansion, characterised by a 15% increase in leaf thickness and a 17% enlargement in mesophyll cell area on Day 1 (Table 3). These dimensional increases, which may occur during the early phase of water deficit before bulk tissue turgor loss is complete, were associated with marked reductions in CO_2 diffusion capacity (21% decrease in f_{ias}, 23% decline in S_c/S). This counterintuitive combination can be explained if initial osmotic adjustment and cell wall loosening in some mesophyll cells transiently maintain or even promote localised expansion, while adjacent cells or tissues begin to lose volume. This differential behaviour could lead to the mechanical compression of intercellular air spaces, creating a physical barrier to gas exchange (Flexas et al. 2012). We note that measurements from 2D sections may

https://doi.org/10.17221/564/2025-PSE

also accentuate the apparent size of remaining cells if surrounding cells collapse. Regardless of the proximate cause, the net structural outcome, a collapse of airspace network, aligns with previous reports of drought-induced mesophyll deformation that compromises CO_2 conductance (Rachana et al. 2024). While the M treatment exhibited rapid restoration of leaf morphology, with 7–26% increases in structural parameters by Day 3, the persistent depression of S_c/S and f_{ias} values below control levels suggests a temporal decoupling between cellular reinflation and the reestablishment of functional airspace networks. This lag implies that the reconstruction of gas diffusion pathways takes longer than simple turgor recovery (Ruehr et al. 2019). More critically, the S treatment showed only transient volumetric recovery, with a 38% rebound in cell volume, without corresponding improvements in S_c/S or f_{ias}, indicating irreversible damage to the chloroplast-airspace interface. This structural failure likely explains the commonly observed photosynthetic non-recovery in severely stressed plants even after rehydration (Xue et al. 2022).

The chloroplast responses to varying levels of drought indicate distinct adaptation strategies. The S treatment caused a significant 52% reduction in total chlorophyll ($a + b$) and a 53% decline in the chlorophyll a/b ratio (Table 4), suggesting preferential degradation of PSII core complexes, consistent with drought-induced oxidative damage mechanisms (Lodeyro et al. 2021, Moustakas et al. 2022). While artificial manipulation of chloroplast size failed to enhance photosynthetic efficiency in tobacco (Gowacka et al. 2023), our observation of compensatory chloroplast expansion under stress suggests that plants transiently modulate organelle morphology as an emergency response. However, such changes likely incur hidden costs (e.g., reduced g_m), reinforcing that naturally evolved chloroplast dimensions may represent an optimal trade-off between structural stability and metabolic function (Gowacka et al. 2023). After rehydration, the M treatment showed a rapid 17% increase in the chlorophyll a/b ratio on Day 3 and 23% chloroplast proliferation on Day 4, indicating efficient reactivation of PSII repair cycles and chloroplast biogenesis (Charuvi et al. 2018). However, the slower recovery of $Area_{chl}$ suggests the formation of smaller chloroplasts during early recovery (Nagy-Deri et al. 2011). This structural-functional decoupling highlights the hierarchical nature of photosynthetic recovery, with pigment-protein complex regeneration preceding organelle ultrastructure restoration (Moustakas et al. 2022, Rachana et al. 2024). In contrast, the S treatment showed a sustained 32% chlorophyll deficit on Day 3 and permanent reductions in chloroplast dimensions after rehydration, indicating a collapse of the chloroplast repair machinery. The transient chlorophyll content rebound on Day 5 likely reflects residual biosynthetic activity rather than functional recovery, as evidenced by the concurrent 22% chloroplast loss and structural deterioration, consistent with terminal senescence processes (Charuvi et al. 2018).

Mechanistic insights into the structural-functional coordination. The strong direct effect of f_{ias} on g_m ($\beta = 0.28$, $P < 0.01$) underscores its role as the primary determinant of gaseous phase resistance in sugar beet. This observation is consistent with diffusion theory and anatomical models of gas-phase conductance, in which the fraction of intercellular airspace (f_{ias}) interacts with tortuosity (τ) and the effective diffusion pathlength (L) to determine resistance (Terashima et al. 2011, Onoda et al. 2017). Notably, the reduction in f_{ias} under severe stress corresponds to an increase in diffusion resistance, explaining the disproportionate decline in g_m. This nonlinear relationship suggests threshold behaviour, below a critical f_{ias} (15% in this study), CO_2 diffusion becomes severely rate-limiting, consistent with observations in cotton (*Gossypium hirsutum*) (Zou et al. 2022). While S_c/S also showed a strong direct effect ($\beta = 0.35$), its mediation of the influence of f_{ias} (indirect effect = 0.18) implies compensatory chloroplast positioning under airspace constraints. For instance, reduced f_{ias} triggers chloroplast repositioning toward cell peripheries *via* actin cytoskeleton remodelling, partially maintaining S_c/S and minimising liquid-phase resistance (Kim et al. 2020). Moreover, the observed 23% reduction in $Area_{chl}$ (Table 4) led to a disproportionate 14% decrease in S_c/S, indicating that changes in cell volume directly drive the remodelling of the chloroplast-airspace interface (Charuvi et al. 2018).

Given the key roles of S_c/S and fias as critical determinants of gaseous-phase resistance in sugar beet, it is essential to explore potential targets that could be manipulated to enhance photosynthetic resilience under water-deficit conditions. The observed 21% reduction in f_{ias} under severe stress (Table 3), translating to a theoretical 34% increase in diffusion resistance, underscores the importance of maintaining mesophyll structural integrity and

https://doi.org/10.17221/564/2025-PSE

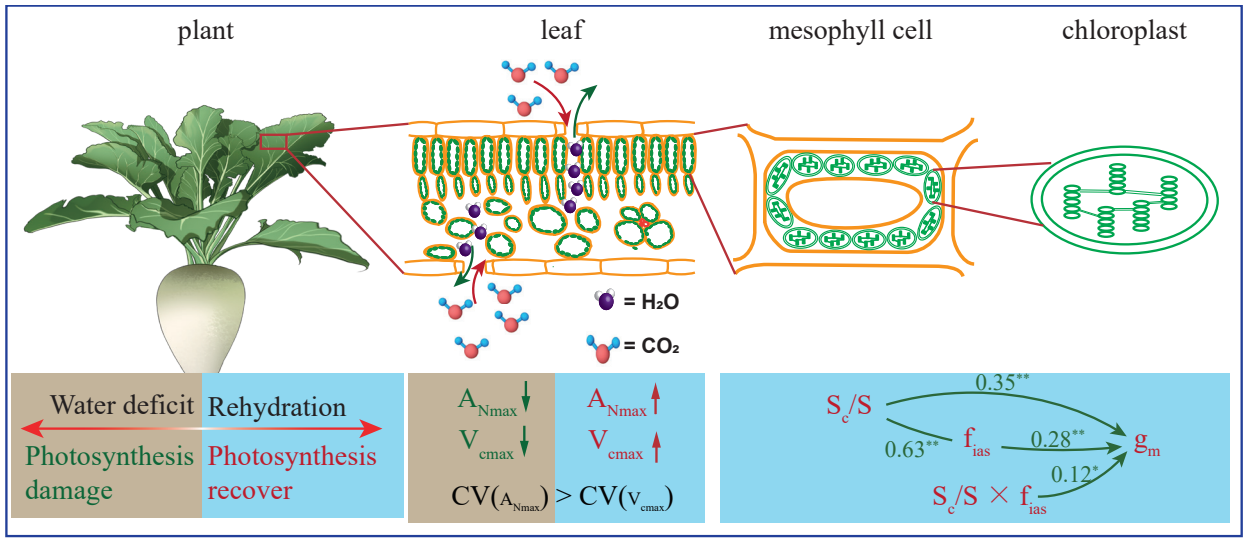

Figure 10. The intricate multiscale mechanisms that underlie the responses of sugar beet to water deficit and rehydration

chloroplast dynamic positioning as critical strategies for improving g_m (Charuvi et al. 2018, Kim et al. 2020). For instance, expansins have been shown to maintain cell wall elasticity, thus preventing the collapse of f_{ias} under drought stress (Cosgrove 2016, 2022). Similarly, reducing cell wall cross-linking is instrumental in preventing compression of intercellular spaces, thereby supporting photosynthetic rates (Aneja et al. 2025). The role of blue light receptors in activating chloroplast avoidance movement to optimise S_c/S further highlights the potential of manipulating light signalling pathways to enhance photosynthetic efficiency (Shang et al. 2018). The regulation of chloroplast movement by proteins like CHUP1 (Kim et al. 2020) and PHOT2 (Shang et al. 2018) also presents an opportunity to fine-tune S_c/S, thereby optimising the chloroplast-airspace interface for efficient gas exchange. Therefore, manipulating structural targets offers a promising avenue to enhance photosynthetic resilience in sugar beet under water-deficit-rehydration conditions (Figure 10).

REFERENCES

Aneja P., Sanyal R., Ranjan A. (2025): Leaf growth in third dimension: a perspective of leaf thickness from genetic regulation to ecophysiology. New Phytologist, 245: 989–999.

Barratt G.E., Sparkes D.L., McAusland L., Murchie E.H. (2020): Anisohydric sugar beet rapidly responds to light to optimize leaf water use efficiency utilizing numerous small stomata. AoB PLANTS, 13: plaa067.

Bloch D., Hoffmann C.M., Märländer B. (2006): Impact of water supply on photosynthesis, water use and carbon isotope discrimination of sugar beet genotypes. European Journal of Agronomy, 24: 218–225.

Brown K.F., Messem A., Dunham R., Biscoe P. (1987): Effect of drought on growth and water use of sugar beet. The Journal of Agricultural Science, 109: 421–435.

Charuvi D., Nevo R., Aviv-Sharon E., Gal A., Kiss V., Shimoni E., Farrant J.M., Kirchhoff H., Reich Z. (2018): Chloroplast breakdown during dehydration of a homoiochlorophyllous resurrection plant proceeds *via* senescence-like processes. Environmental and Experimental Botany, 157: 100–111.

Chaves M.M., Flexas J., Pinheiro C. (2009): Photosynthesis under drought and salt stress: regulation mechanisms from whole plant to cell. Annals of Botany, 103: 551–560.

Cosgrove D.J. (2016): Plant cell wall extensibility: connecting plant cell growth with cell wall structure, mechanics, and the action of wall-modifying enzymes. Journal of Experimental Botany, 67: 463–476.

Cosgrove D.J. (2022): Building an extensible cell wall. Plant Physiology, 189: 1246–1277.

Dohm J.C., Minoche A.E., Holtgräwe D., Capella-Gutiérrez S., Zakrzewski F., Tafer H., Rupp O., Sörensen T.R., Stracke R., Reinhardt R. (2014): The genome of the recently domesticated crop plant sugar beet (*Beta vulgaris*). Nature, 505: 546–549.

Evans J.R., Caemmerer S.V., Setchell B.A., Hudson G.S. (1994): The relationship between CO_2 transfer conductance and leaf anatomy in transgenic tobacco with a reduced content of Rubisco. Australian Journal of Plant Physiology, 21: 475–495.

Farquhar G.D., Caemmerer S.V., Berry J.A. (1980): A biochemical model of photosynthetic CO_2 assimilation in leaves of C3 species. Planta, 149: 78–90.

Fitters T.F., Mooney S.J., Sparkes D.L. (2022): Impact of water availability on root growth of sugar beet varieties. Soil Use and Management, 38: 1033–1043.

https://doi.org/10.17221/564/2025-PSE

Flexas J., Barbour M.M., Brendel O., Cabrera H.M., Carriquí M., Diaz-Espejo A., Douthe C., Dreyer E., Ferrio J., Juan P., Galle A., Galmés J., Kodama N., Medrano H., Niinemets Ü., Peguero Pina J.J., Pou A., Ribas-Carbo M., Tomas M., Tosens T., Warren C.R. (2012): Mesophyll diffusion conductance to CO_2: an unappreciated central player in photosynthesis. Plant Science (Amsterdam, Netherlands), 193: 70–84.

Flexas J., Carriquí M. (2020): Photosynthesis and photosynthetic efficiencies along the terrestrial plant's phylogeny: lessons for improving crop photosynthesis. The Plant Journal, 101: 964–978.

Flexas J., Fernie A., Usadel B., Alonso-Forn D., Ardiles V., Ball M., Ballesteros D., Bravo L., Brodribb T., Carriquí M., Castanyer-Mallol F., Cavieres L., Chondol T., Clemente-Moreno M., Coopman R., Corcuera L., De Vries J., Diaz-Espejo A., Dolezal J., Ergo V., Fernández H., Fernández-Marín B., Galmes J., García-Plazaola J., Quintanilla L., Gulías J., Hernández A., Luo K1, Martínez-Abaigar J., Nadal M., Niinemets Ü., Núñez-Olivera M., Ostria-Gallardo E., Perera, Castro A., Pérez-López U., Ribas-Carbo M., Roig-Oliver M., Rojas R., Sáez P., Tosens T., Viveros R., Xiong D., Yan J., Zhang Y., Gago J. (2025): What can we learn from the ecophysiology of plants inhabiting extreme environment. Journal of Experimental Botany, 76: eraf236.

Flexas J., Matilde B., Josefina B., Jean-Marc D., Alexander G., Jeroni G., Miguel J., Alícia P., Miquel R.-C., Carlota S. (2009): Photosynthesis limitations during water stress acclimation and recovery in the drought-adapted *Vitis* hybrid Richter-110 (*V. berlandieri* × *V. rupestris*). Journal of Experimental Botany, 60: 2361–2377.

Galle A., Florez-Sarasa I., Tomas M., Pou A., Medrano H., Ribas-Carbo M., Flexas J. (2009): The role of mesophyll conductance during water stress and recovery in tobacco (*Nicotiana sylvestris*): acclimation or limitation? Journal of Experimental Botany, 60: 2379–2390.

Ghaffari H., Tadayon M.R., Bahador M., Razmjoo J. (2021): Investigation of the proline role in controlling traits related to sugar and root yield of sugar beet under water deficit conditions. Agricultural Water Management, 243: 106448.

Gowacka K., Kromdijk J., Salesse-Smith C.E., Smith C., Driever S.M., Long S.P. (2023): Is chloroplast size optimal for photosynthetic efficiency? New Phytologist, 239: 2197–2211.

Grassi G., Magnani F. (2005): Stomatal, mesophyll conductance and biochemical limitations to photosynthesis as affected by drought and leaf ontogeny in ash and oak trees. Plant Cell and Environment, 28: 834–849.

Hair J.F., Hult G.T.M., Ringle C.M., Sarstedt M. (2022): A Primer on Partial Least Squares Structural Equation Modeling (PLS-SEM). 3rd Edition. Sage, Thousand Oaks.

Harley P.C., Loreto F., Di Marco G., Sharkey T.D. (1992): Theoretical considerations when estimating the mesophyll conductance to CO_2 flux by analysis of the response of photosynthesis to CO_2. Plant Physiology, 98: 1429–1436.

Kim J.Y., Ahn J., Bong H., Wada M., Kong S.G. (2020): *ACTIN2* functions in chloroplast photorelocation movement in *Arabidopsis thaliana*. Journal of Plant Biology, 63: 379–389.

Lodeyro A.F., Krapp A.R., Néstor C. (2021): Photosynthesis and chloroplast redox signaling in the age of global warming: stress tolerance, acclimation and developmental plasticity. Journal of Experimental Botany, 72: 5919–5937.

Moustakas M., Sperdouli I., Moustaka J. (2022): Early drought stress warning in plants: color pictures of photosystem II photochemistry. Climate, 10: 179.

Nagy-Deri H., Péli E.R., Georgieva K., Tuba Z. (2011): Changes in chloroplast morphology of different parenchyma cells in leaves of *Haberlea rhodopensis* Friv. during desiccation and following rehydration. Photosynthetica, 49: 119–126.

Niinemets Ü., Reichstein M. (2003): Controls on the emission of plant volatiles through stomata: a sensitivity analysis. Journal of Geophysical Research: Atmospheres, 108: SOS 5-1-SOS 3-11.

Onoda Y., Wright I.J., Evans J.R., Hikosaka K., Kitajima K., Niinemets Ü., Poorter H., Tosens T., Westoby M. (2017): Physiological and structural tradeoffs underlying the leaf economics spectrum. New Phytologist, 214: 1447–1463.

Rachana O., Takao O., Daisuke S., Mitsutaka T. (2024): Structural changes of mesophyll cells in the rice leaf tissue in response to salinity stress based on the three-dimensional analysis. AoB PLANTS, 16: plae016.

Ruehr N.K., Rüdiger G., Stefan M., Almut A. (2019): Beyond the extreme: recovery of carbon and water relations in woody plants following heat and drought stress. Tree Physiology, 39: 1285–1299.

Sagardoy R., Vázquez S., Florez-Sarasa I., Albacete A., Ribas-Carbó M., Flexas J., Abadía J., Morales F. (2010): Stomatal and mesophyll conductances to CO_2 are the main limitations to photosynthesis in sugar beet (*Beta vulgaris*) plants grown with excess zinc. New Phytologist, 187: 145–158.

Sahin U., Ors S., Kiziloglu F.M., Kuslu Y. (2014): Evaluation of water use and yield responses of drip-irrigated sugar beet with different irrigation techniques. Chilean Journal of Agricultural Research, 74: 302–310.

Shaaban A., Abdou N.M., Elmageed T.A.A., Semida W.M., Tawwab A.R.A.E., Mohamed G.F., Mohamed M.S., Elsaadony M.T., El-Tarabily K.A., Abuqamar S.F. (2025): Foliar fertilization with potassium silicate enhances water productivity and drought resilience in sugar beet. Field Crops Research, 326: 109840.

Shang B., Zang Y., Zhao X., Zhu J., Zhang X. (2018): Functional characterization of *GhPHOT2* in chloroplast avoidance of *Gossypium hirsutum*. Plant Physiology and Biochemistry, 135: 51–60.

Sharkey T.D. (2016): What gas exchange data can tell us about photosynthesis. Plant Cell and Environment, 39: 1161–1163.

Syvertsen J.P., Lloyd J., McConchie C., Kriedemann P.E., Farquhar G.D. (1995): On the relationship between leaf anatomy and CO_2

https://doi.org/10.17221/564/2025-PSE

diffusion through the mesophyll of hypostomatous leaves. Plant, Cell and Environment, 18: 149–157.

Terashima I., Hanba Y.T., Tholen D., Niinemets Ü. (2011): Leaf functional anatomy in relation to photosynthesis. Plant Physiology, 155: 108–116.

Thain J.F. (1983): Curvature correction factors in the measurement of cell surface areas in plant tissues1. Journal of Experimantal Botany, 34: 87–94.

Tomás M., Jaume F., Lucian C., Jeroni G., Lea H., Hipólito M., Miquel R.-C., Tiina T., Vivian V., Ülo N. (2013): Importance of leaf anatomy in determining mesophyll diffusion conductance to CO_2 across species: quantitative limitations and scaling up by models. Journal of Experimental Botany, 64: 2269–2281.

Tosens T., Nishida K., Gago J., Coopman R.E., Cabrera H.M., Carriquí M., Laanisto L., Morales L., Nadal M., Rojas R., Talts E., Tomas M., Hanba Y., Niinemets Ü., Flexas J. (2016): The photosynthetic capacity in 35 ferns and fern allies: mesophyll CO_2 diffusion as a key trait. New Phytologist, 209: 1576–1590.

Tsai M.Y., Kuan C., Guo Z.L., Yang H.A., Chung K.F., Ho C.K. (2022): Stomatal clustering in Begonia improves water use efficiency by modulating stomatal movement and leaf structure. Plant-Environment Interactions, 3: 141–154.

Velikova V., Tsonev T., Tattini M., Arena C., Krumova S., Koleva D., Peeva V., Stojchev S., Todinova S., Izzo L.G., Brunetti C., Stefanova M., Taneva S., Loreto F. (2018): Physiological and structural adjustments of two ecotypes of *Platanus orientalis* L. from different habitats in response to drought and re-watering. Conservation Physiology, 6: coy073.

Von Caemmerer S. (2000): Biochemical models of leaf photosynthesis. Collingwood, Csiro Publishing.

Xue S., Zang Y., Chen J., Shang S., Tang X. (2022): Effects of enhanced UV-B radiation on photosynthetic performance and non-photochemical quenching process of intertidal red macroalgae *Neoporphyra haitanensis*. Environmental and Experimental Botany, 199: 104888.

Yamori W., Suzuki K., Noguchi K.O., Nakai M., Terashima I. (2006): Effects of Rubisco kinetics and Rubisco activation state on the temperature dependence of the photosynthetic rate in spinach leaves from contrasting growth temperatures. Plant, Cell and Environment, 29: 1659–1670.

Zou J., Hu W., Li Y., Zhu H., He J., Wang Y., Meng Y., Chen B., Zhao W., Wang S. (2022): Leaf anatomical alterations reduce cotton's mesophyll conductance under dynamic drought stress conditions. The Plant Journal, 111: 391–405.

Received: December 15, 2025
Accepted: January 15, 2026
Published online: January 27, 2026